

# Mechanical behaviors of concrete-filled rectangular steel tubular under pure torsion

Fa-xing Ding<sup>1,2</sup>, Shi-jing Sheng<sup>1</sup>, Yu-jie Yu<sup>\*1</sup> and Zhi-wu Yu<sup>1</sup>

<sup>1</sup> School of Civil Engineering, Central South University, Changsha 410075, P.R. China

<sup>2</sup> Engineering Technology Research Center for Prefabricated Construction Industrialization of Hunan Province, Changsha 410075, P.R. China

(Received November 2, 2018, Revised March 5, 2019, Accepted April 5, 2019)

**Abstract.** Pure torsion loading conditions were not frequently occurred in practical engineering, but the torsional researches were important since it's the basis of mechanical property researches under complex loading. Then a 3D finite element model with precise material constitutive models was established, and the effectiveness was verified with test data. Parametric studies with varying factors as steel yield strength, concrete strength and sectional height-width ratio, were performed. Internal stress state and the interaction effect between encased steel tube and the core concrete were analyzed. Results indicated that due to the confinement effect between steel tube and core concrete, the torsional strength of CFT columns was greatly improved comparing to plain concrete columns. The steel ratio would greatly influence the torque share between the steel tube and the core concrete. Then the torsional strength calculation formulas for core concrete and the whole CFT column were proposed. The proposed formula could be simpler and easier to use with guaranteed accuracy. Related design codes were more conservative than the proposed formula, but the proposed formula presented more satisfactory agreement with experimental results.

**Keywords:** concrete-filled steel tube (CFT); pure torsion; finite element analysis; torsional bearing capacity; section shearing stiffness

## 1. Introduction

The concrete filled tubular (CFT) possesses high compressive strength and good ductility due to the corporative working effect between steel tube and core concrete. The confinement effect from encased steel tube to the infilled concrete can well exerted the compressive strength of concrete and high tensile strength of steel tube (Abed *et al.* 2013, Lai and Ho 2014, Evirgen *et al.* 2014). The CFT columns have already been widely used as an important structural member, then the mechanical properties received lots of researches in past decades. Previous researches on CFT column included the strength calculation and deforming ability under compression load, bending load, shear load and their combinations as hybrid loading conditions (Xiamuxi and Akira 2011, Moon *et al.* 2012, Kim *et al.* 2013, 2015, Park and Choi 2013, Mashiri *et al.* 2014, Uenaka and Tsunokake 2016, Patel *et al.* 2016). And the researching subjects were mainly around tubular and square section columns based on the high frequency applications of these members. In actual engineering applications, pure torsion conditions were rare for the CFT members. And the torsion load was often induced in combination with compression, bending or shear load. However, the pure torsion properties are the basis of mechanical behaviors of CFT columns under complex or

hybrid loads. And the presence of torque effect often facilitated the early failure of frame columns, or increases the difficulties on predicting the column capacity under earthquake excitations. Also, when CFT columns are applied to the curved girder bridge, piers are not only subjected to axial force and bending moment, but also subjected to torsion. It was found in many previous earthquake disaster investigations that this kind of bridge structure was seriously damaged under earthquake (Wang 2013). Therefore, the mechanical behavior of CFT columns under pure torsion is still necessary. At present, the researches on the torsion properties were mainly around the circular CFT columns. Beck conducted experimental studies on circular section CFT members under pure torsion and found that the torsional bearing ability was improved dramatically than that of hollow section steel tube. And this strengthening effect mainly came from the local buckling prevention at steel tube from the constraining effect of infilled concrete (Beck and Kiyomiya 2003). Gong (1989) and Lee *et al.* (2009) have carried out testes on circular section CFT members under pure static torsion, and investigated the joint working mechanism between encased steel tube and confined concrete. Then Han *et al.* (2007a, b) proposed a three-dimensional refined FE model, and then applied the model to investigate the nonlinear torsion behavior of different kind CFT members. Ding *et al.* (2018) also discussed the mechanical behavior and pure torsion design method of circular CFT column through 3D finite element modelling method. Comparing to pure torsion researches on circular CFT members, related tests and

\*Corresponding author, Professor,  
E-mail: [yujiecsu@csu.edu.cn](mailto:yujiecsu@csu.edu.cn)

discussions on rectangular section columns were limited, most of which even focused on square section ones. Nie *et al.* (2012) carried out a series of tests on CFT columns that subjected to pure torsion, axial compression with torsion and bending with torsion loads. Both circular section and rectangular section columns were considered and results indicated that the failure modes, and strength development and degradation under combined torsion due to different corporative working mechanisms. Chen (2003) once experimented 1 square and 2 rectangular CFT columns under pure torsion, and found that no relative slips were presented between steel tube and core concrete under pure torsion. Kitada (1991) carried out experimental research on a CFT short column member with square section under pure torsion, and made a contrastive study of hollow steel tube and short concrete columns. Wang *et al.* (2016) carried out an experimental study on CFT column with rectangular section that subjected to compression-flexure-torsion combined action and then proposed a nonlinear fiber beam modelling method.

The in-depth investigation of torsion properties can help ensure the reasonable and safe design of CFT column. But since specific torsion test investigations on rectangular CFT columns were limited, and present torsion researches mainly referred to that of circular and square columns. There are still several questions remained for rectangular CFT columns. For instance, previous experimental and numerical investigations mainly adopted reduced scale models, without further considerations on the mechanical differences comparing to the full-scale columns. Moreover, the corporative working mechanism, confinement effect, and the torsion load share ration between steel tube and infill concrete under torque load were different between rectangular and circular CFT columns due to the different section constructions. Although those properties are important for the overall torsion performance, and constitute the basic principle for torsion strength calculations, relative discussions are still limited.

Therefore, in this paper, a systematic investigation was performed on the pure torsion behavior of rectangular CFT columns through finite element modelling approach. Refined FE models were established with reasonable and precise material constitutive models. Then the joint working mechanism and confinement effect between steel tube and

infill concrete were investigated through parametric studies. A modified formula for pure torsion strength calculation was proposed based on the discussions and then the effectiveness was compared with existing codes.

## 2. Finite element modelling

### 2.1 Finite element modelling

Many researches have validated that the mechanical performance of CFT columns can be well predicted through refined FE modeling with proper settings (Han *et al.* 2007a, Hassanein and Kharoob 2014, Aslani *et al.* 2016, Ding *et al.* 2018). Here ABAQUS version 6.14 software was used in this paper for the torsional simulation of rectangular CFT columns. The 8-node 3D solid element with reduced integration (C3D8R) was adopted to model the core concrete, the steel tube and the loading plate. Round angle edge of rectangular section was also established in the FE model to reflect the practical member construction. The surface-to-surface contact was chosen for the constraint between steel tube and core concrete, with the inner surface of steel tube being the “MASTER” face and the external surface of core concrete being the “SLAVE” face. “HARD CONTACT” mode was adopted for the nominal direction tangential behavior to simulate the bond-slip action between steel tube and core concrete. A friction coefficient of 0.5 was selected with referring to previous researches (Ding *et al.* 2018). The established model is shown in Fig. 1. The concrete material model adopted the damage plasticity concrete model with a stress-strain relation fitted out from multi-axial loading condition. And the steel material model used the combined hardening with Von Mises criteria constitutive model. Detailed material parameter determination process and effectiveness validation process can be found in references (Ding *et al.* 2011, 2018).

### 2.2 Model validation

The experimental investigations on concrete-filled steel tubes under pure torsion that presented previously (Kitada 1991, Chen 2003) were used to verify the developed FE



Fig. 1 Established FE model of rectangular CFT columns under pure torsion

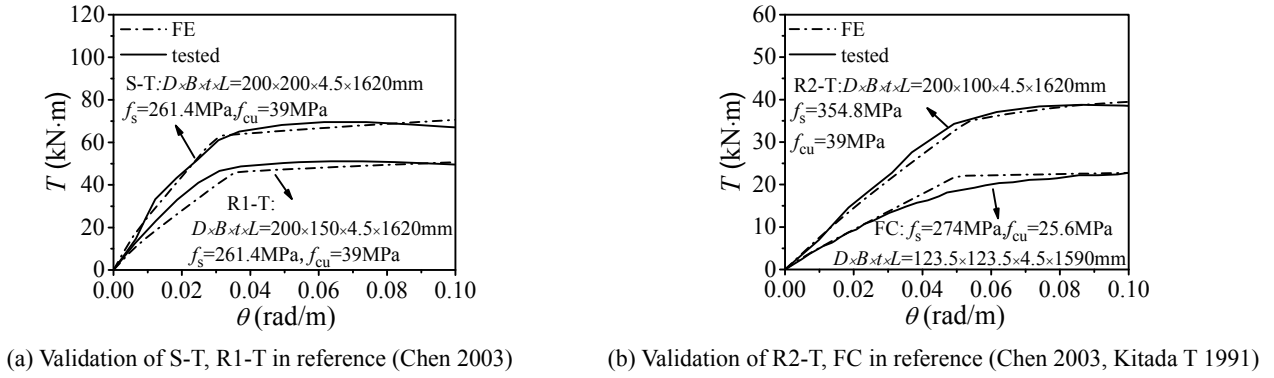


Fig. 2 Comparison of  $T$ - $\gamma$  curves between FE results, tested results

model. Fig. 2 gives the results obtained from FE simulations and test data, where  $D$  is the section height,  $B$  is the section width,  $t$  is wall thickness of the steel tube and  $L$  is the length of CFT columns respectively. The comparisons indicated that the FE model can precisely reflect the torsional strength development and degradation process. The torsional bearing process can be divided into three stages, namely elastic stage, elastic-plastic stage and the plastic degradation stage. And given  $T_{u,c}$  as the ultimate torsion strength from the tests, and  $T_{u,0}$  as the FE strengths. The mean value of the ultimate strength ratio  $T_{u,c}/T_{u,0}$  was 1.05, with the corresponding coefficients of variation (COV) of 0.01. Then the FE model was adequately predicted the ultimate torsional strength of CFT columns, and was subsequently used for further parametric studies to investigate the joint working mechanism of rectangular CFT member under pure torsion.

### 2.3 Parametric study

With the verified FE model, parameters affecting the torsion strength development of rectangular CFT columns were studied. Fig. 3 shows torsion moment ( $T$ ) versus sectional maximum shearing strain ( $\gamma$ ) curves of rectangular CFT columns extracted by ABAQUS. In this paper,  $\gamma$  is shearing strain at the verge center on the middle section. The investigated parameters contained steel yield strength ( $f_s$ ), concrete strength ( $f_{cu}$ ), steel ratio ( $\rho$ ), section height ( $D$ ), section width ( $B$ ) and column length ( $L$ ). Models of full scale CFT columns were established, and a total of 39 models were analyzed in the parametric study. The basic calculating conditions were:  $D/B = 1.5$  ( $B = 400$  mm),  $L = 2000$  mm,  $f_{cu} = 40$  MPa,  $f_s = 235$  MPa,  $\rho = 0.05$ .

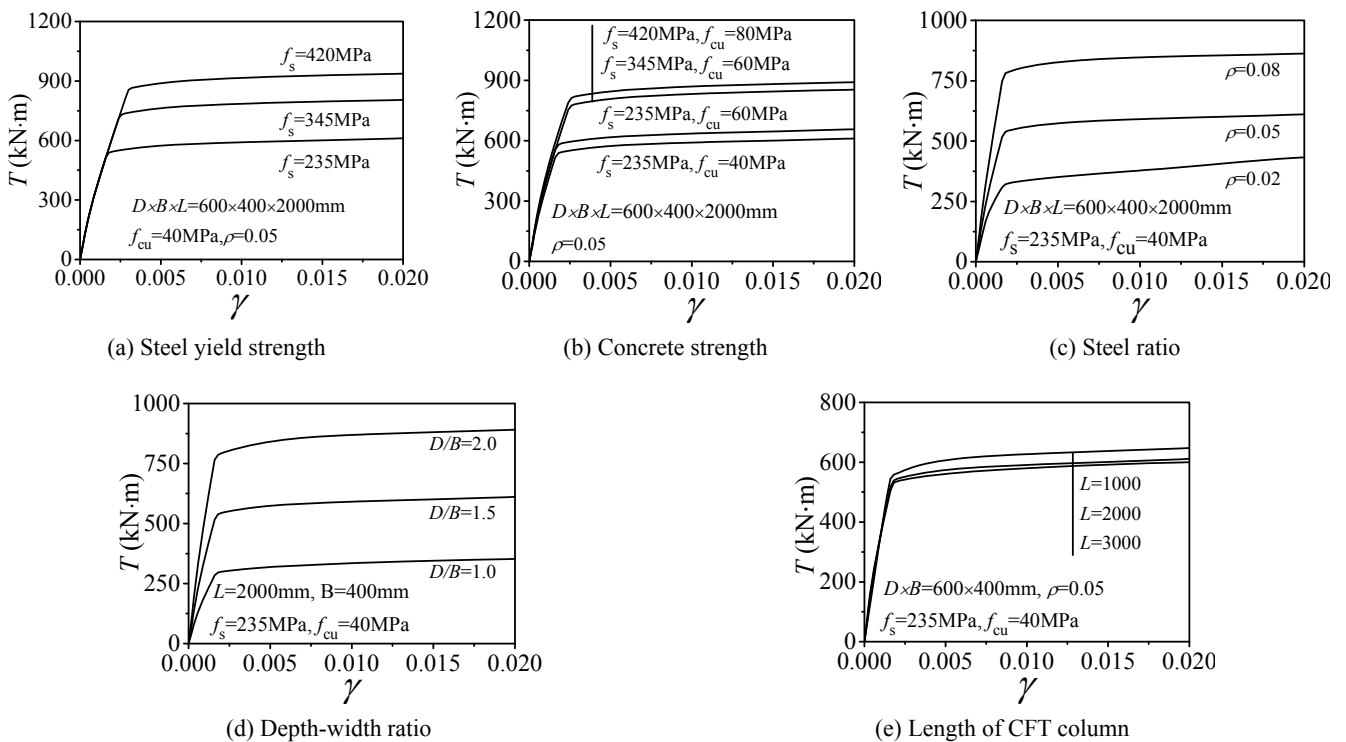


Fig. 3 Parametric analysis on  $T$ - $\gamma$  curves

### 2.3.1 Steel yield strength ( $f_s$ )

Fig. 3(a) presents  $T$ - $\gamma$  curves of rectangular CFT columns with steel yield strength ( $f_s$ ) varying from Q235 to Q420. It indicated that  $f_s$  had little effect on the elastic stiffness. Since the section construction of the columns, and the material modulus were still the same between different grade steels. The steel yield strength mainly influenced the ultimate torsional moment. Comparing to the specimen with Q235 steel, the ultimate torsional moment was improved by 17% for specimen with Q345 steel, and was improved by 33% for specimen with Q420 steel.

### 2.3.2 Concrete strength ( $f_{cu}$ )

Fig. 3(b) gives the  $T$ - $\gamma$  curves of models with different concrete strength ( $f_{cu}$ ). The concrete strength still present little influence on the elastic stiffness, but displayed weak effect on the ultimate torsional moment. With the same steel grade (Q235 or Q345), the ultimate torsional strength only increased by 8% as the increase of concrete strength.

### 2.3.3 Steel ratio ( $\rho$ )

Fig. 3(c) compares the  $T$ - $\gamma$  curves of rectangular CFT columns with steel ratio ( $\rho$ ) varying from 0.02 to 0.08. It was shown that the composite torsional stiffness was increased as the increase of steel ratio. While the increasing speed slowed down in high  $\rho$  conditions. Comparing to 0.02 steel ratio case, the ultimate torsional moment was improved by 63% in 0.08 steel ratio case, and increased by 44% in 0.05 steel ratio case. Therefore, the steel ratio was a primary influencing factor on the ultimate torsional capacity of the CFT columns.

### 2.3.4 Depth-width ratio ( $D/B$ )

Fig. 3(d) compares the  $T$ - $\gamma$  curves of rectangular CFT columns with steel ratio ( $\rho$ ) varying from 0.02 to 0.08. It was shown that the composite torsional stiffness was increased as the increase of steel ratio. While the increasing speed slowed down in high  $\rho$  conditions. Comparing to 0.02 steel ratio case, the ultimate torsional moment was improved by 63% in 0.08 steel ratio case, and increased by 44% in 0.05 steel ratio case. Therefore, the steel ratio was a primary influencing factor on the ultimate torsional capacity of the CFT columns.

### 2.3.5 Length of CFT column ( $L$ )

Fig. 3(e) presents the  $T$ - $\gamma$  curves of rectangular CFT

columns with different length ( $L$ ). Results indicated that the torsional strength had little effect among columns with different lengths. In previous researches (Ding *et al.* 2018), the parametric investigation on the torsional strength of circular CFT columns were performed, and the factor influencing patterns were found similar between rectangular CFT columns and circular CFT columns.

## 2.4 The confinement effect discussion

Except for the factor influencing patterns, the confinement effect between the steel tube and the core concrete was also discussed to further understand the corporative working mechanisms under torque load. Here the basic calculating case was settled as:  $D/B = 0.5$  ( $B = 400$  mm),  $L = 2000$  mm,  $\rho = 0.05$ ,  $f_s = 235$  MPa,  $f_{cu} = 40$  MPa.

### 2.4.1 The confinement effect to steel tube

Fig. 4 shows the typical failure mode of the steel tube in a rectangular CFT column, and the failure state of corresponding hollow section steel tube (HST) under pure torsion. Obvious differences were presented between the torsional failure mode of CFT and HST members. The HST column had relative weak local buckling stability at constituted plates, and presented local depression deformation under the 45-degree principal compressive stress resulted from pure torsion. Then finally, the HST column failed with plastic hinge development. While for the CFT columns, the inner concrete can provide support and constraining effect to the steel tube plates, and then obvious local buckling was prevented. Then CFT column displayed steady torsion load bearing behavior and material plastic strength development.

Fig. 5 provides the  $T$ - $\gamma$  curves of steel tube under pure torsion from both the CFT column and HST column. The comparison indicated that the two curves were quite similar. The stress state in the steel tube of CFT column was mainly biaxial state, and the steel tube also bear the axial tension stress that resulted from the deformation of core concrete (Gong 1989). Furthermore, the steel tube in CFT columns had higher stability due to the local buckling resisting effect from the core concrete. Therefore, the  $T$ - $\gamma$  curve of the steel tube in CFT column displayed little degradation and strength descending behaviors. Han *et al.* (2007b) once performed experimental and numerical studies on the torsional strength of circular and square CFT columns, and proposed a method to determine the ultimate strength. Then



Fig. 4 Typical failure modes of steel tube in CFT column and HST

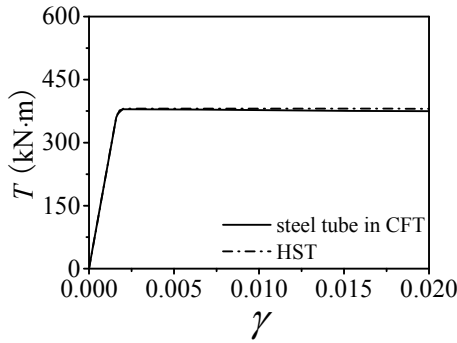


Fig. 5 Comparisons between the steel tube in CFT column and the corresponding HST

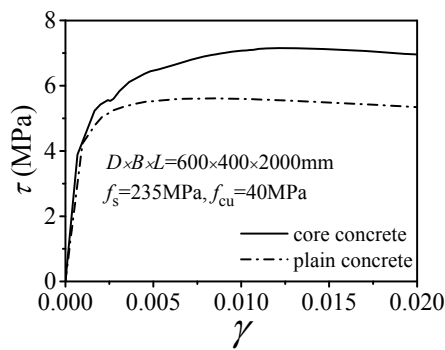


Fig. 6 Comparison of  $\tau$ - $\gamma$  curves between the core concrete and the plain concrete

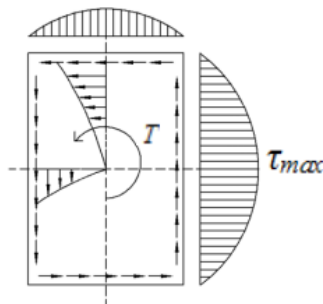


Fig. 7 The shear stress distribution of concrete under pure torsion

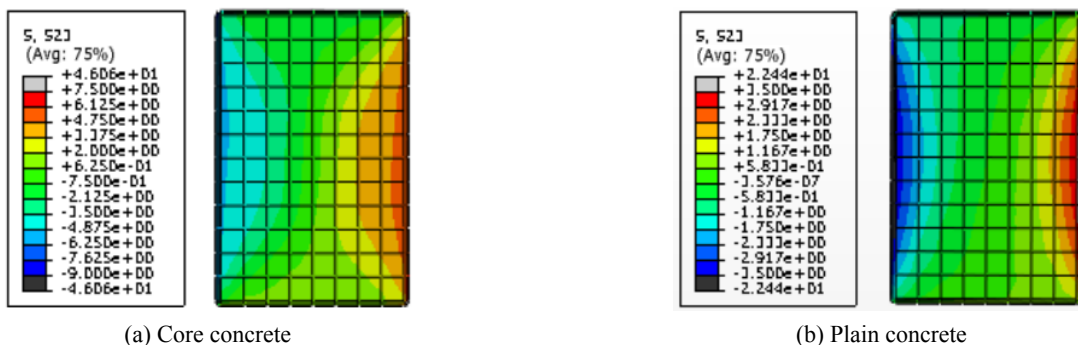
the same strength defining method was adopted here, that the state when the ultimate shear strain ( $\gamma_{sc,u}$ ) in the rectangular CFT column reaching  $10000 \mu\epsilon$  was defined as the ultimate state. And the corresponding torsional moment was determined as the ultimate torsional bearing capacity of the rectangular CFT columns in this paper. Then the ultimate torsional strengths of simulated CFT columns were obtained. Results indicated that the ultimate torsional strength of steel tube from rectangular CFT columns was nearly the same as that in HST column, with merely  $\pm 3\%$  difference. Then it was assumed that the torsional strength of steel tube in CFT column can be estimated from the torsional simulation of HST column with the same section dimension, although with different deformation patterns.

2.4.2 The confinement effect to core concrete

In this section, a pure concrete column with the same dimension of core concrete in CFT columns were analyzed as the comparison. Fig. 6 gives the maximum shear stress ( $\tau$ ) vs. shear strain ( $\gamma$ ) curves that obtained from the core concrete ( $\tau_{cc}$ ) and the pure concrete column ( $\tau_c$ ) under torsion. It presented that compared with plain concrete column, the torsional bearing capacity and the ductility of core concrete were improved distinctly, due to the confinement effect from encased steel tube and the top cover plate. Fig. 7 presents the shear stress distribution at core concrete in the CFT column, and results indicated that the shear stress was maximum at the midpoint of the long side, and was nearly 0 at the corner points. The comparison of the shear stress contours of core concrete and plain concrete column at the failure stage is given in Fig. 8. Similar shear stress distributions were presented, but the core concrete presented higher stress levels than the plain concrete column.

Since compression-torsion combined loading conditions occurred frequently, torsional loading simulations of rectangular CFT columns under different axial compression ratio ( $N/N_u$ ) were performed. And the varying conditions of interaction stress ( $\sigma_{cp}$ ), the normal contact stress between the core concrete and the steel tube, are given in Fig. 9.

Both interaction stress at the center point of long column side, and the stress at column corners were obtained. Results indicated that the rectangular CFT column presented high contact stress  $\sigma_{cp}$  and confinement effect at the corner points, and quite small contact stress at the midspan of section height. The interaction stress  $\sigma_{cp}$



(a) Core concrete

(b) Plain concrete

Fig. 8 Shear stress contours of core concrete and plain concrete

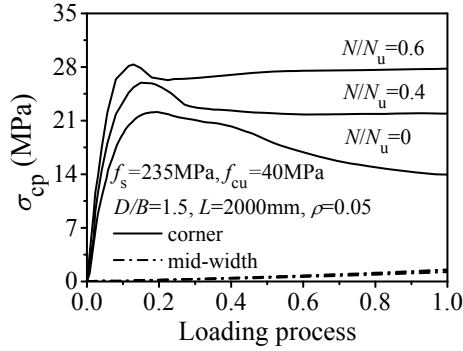


Fig. 9  $\sigma_{cp}$  of rectangular sections with different axial compression ratio

presented linear increase at the initial loading stage, so did the confinement effect and  $\tau_{cc}$  at the core concrete. As the loading continued, the increasing speed of shear stress at core concrete and confinement effect gradually slowed down, and then experienced quick decrease. The ultimate contact stress under 0.4 and 0.6 axial compression ratio cases were about 1.17 times and 1.28 times of the ultimate stress state under none axial compression case. And reasons for this stress elevation mainly came from the triaxial stress state at core concrete resulted from the compression load. Then the compression strength of core concrete was increased, and the shear strength of core concrete during compression-torsion state was increased.

### 3. Design rule discussion

#### 3.1 Shear stress of the core concrete

Above discussions indicated that the core concrete had higher stress levels comparing to plain concrete column under the same loading condition. Then torsional shear strength calculation that applied for plain concrete columns were no longer applicable for rectangular CFT columns, and a modified formula was needed. Then parameter analysis of the affecting ration  $\tau_{cc}/\tau_c$  was conducted based on the validated FE modelling approach. Fig. 10 gives the affection ratio  $\tau_{cc}/\tau_c$  conditions under different steel yield strength  $f_s$ , core concrete strength  $f_{cu}$ , and different sectional Depth-width ratio ( $D/B$ ). Results indicated that as the steel ratio increased from 0.02 to 0.08, the  $\tau_{cc}/\tau_c$  ratio also got increased proportionally from 1.187-1.48. Furthermore, the steel yield strength, core concrete strength and depth-width ratio presented minimum influence on the  $\tau_{cc}/\tau_c$  ratio. The influence range of  $f_s$  and  $f_{cu}$  was less than 5%, and that of  $D/B$  is less than 10%. Then the steel ratio was the primary factor affecting the maximum shear stress of core concrete.

Fig. 11 presents the curve fitting for the  $\tau_{cc}/\tau_c$ - $\rho$  relations of the core concrete in rectangular CFT columns. In order to improve the accuracy of the fitting formula, FE models with 0.01, 0.12 and 0.15 steel ratio were also added in this paper.

Then the calculation formula of  $\tau_{cc}$  can be expressed as

$$\tau_{cc} = (1 + 1.2\rho^{0.4})\tau_c \quad (1)$$

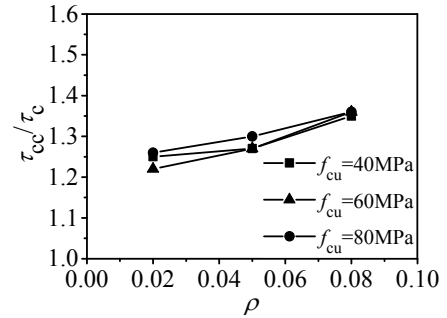
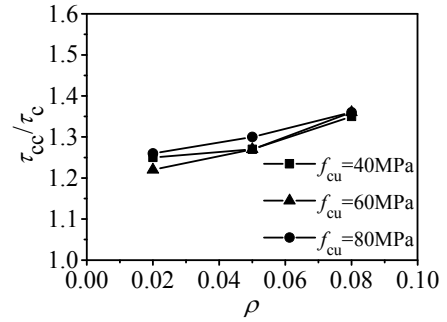
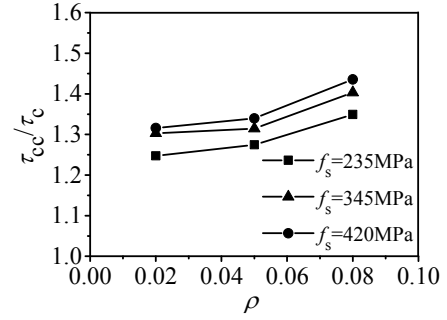


Fig. 10 Parameters studies of  $\tau_{cc}/\tau_c$ - $\rho$  relation

And the curve fitting for  $\tau_c f_{cu}$  relations of the plain concrete column is given in Fig. 12, and the expression can be expressed as

$$\tau_c = 0.56 f_{cu}^{0.62} \quad (2)$$

#### 3.2 Composite shear stiffness under torsion

In the design code GB50936-2014 (2014) and CECS28-2012 (2012), the shear stiffness of composite members was typically computed using the following equation.

$$G_{sc}A_{sc} = G_s A_s + G_c A_c \quad (3)$$

where,  $G_{sc}A_{sc}$  is the composite shear stiffness,  $G_{sc}$  is the nominal composite shear modulus.  $G_s$  and  $G_c$  are the shear modulus of the steel and the concrete,  $A_{sc}$  is the section area,  $A_s$  and  $A_c$  are the area of the steel tube and the concrete. According to previous researches (Ding *et al.* 2011), the composite shear stiffness of CFT columns could be defined as the secant stiffness at the  $0.4\tau_u$  shear stress at  $\tau$ - $\gamma$  curve ( $\tau = T/W_{sc}$ ,  $W_{sc}$  is the torsional section factor,  $W_{sc} = ahb^2$ ,  $a$  is the coefficient related to the  $D/B$  (Liu 2017) and listed in Table 1. and  $\tau_u$  is the maximal shear stress). And then the rectangular CFT column could be considered as a unified

Table 1 The value of  $\alpha$ 

$D/B$	1.0	1.2	1.5	2.0	2.5	3.0	4.0	6.0	8.0	10.0	$\infty$
$\alpha$	0.208	0.219	0.231	0.246	0.258	0.267	0.282	0.299	0.307	0.313	0.333

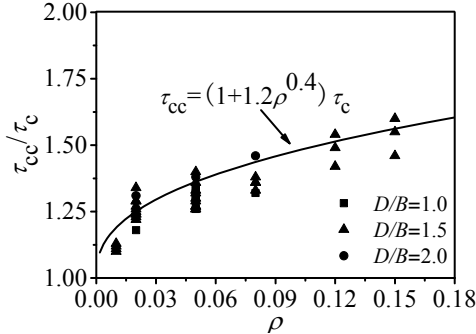
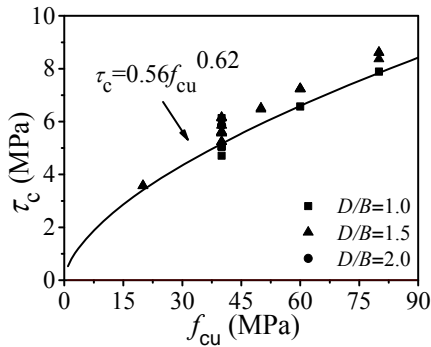

 Fig. 11 Regression results of  $\tau_{cc}/\tau_c \sim \rho$  relation


Fig. 12 Comparison of predicted and tested values

member with composite stiffness.

Fig. 13 shows the comparison of the  $\tau$ - $\gamma$  curves of the whole rectangular CFT column and the core concrete under pure torsion. When  $\tau$  reached  $0.4\tau_u$ , the CFT column and the core concrete stayed at elastic stage, which proved the reasonability of composite stiffness definition. The composite stiffness that obtained from the 39 FE models and corresponding calculated stiffness with Eq. (3) are given in Fig. 14. The comparison indicated that the FE values ( $G_{sc,0}A_{sc}$ ) could well be predicted by the stiffness calculation formula, and the elastic stiffness of the rectangular CFT columns suffered little by the section dimensions.

### 3.3 Ultimate torsional strength

#### 3.3.1 Proposed modified formulas

Based on above discussion, the steel tube and core concrete worked well together, and the ultimate torsional strength can be calculated by directly adding the individual torsional strength of encased steel tube and core concrete. The torsional strength of steel tube can be obtained from the torsional strength calculation of hollow section steel tube, and the torsional strength of core concrete could also be obtained from the plain concrete column. The torsional strength calculation of rectangular CFT columns was expressed as

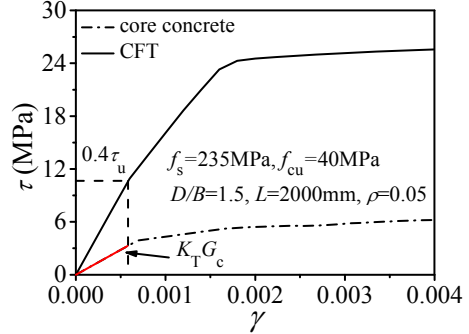
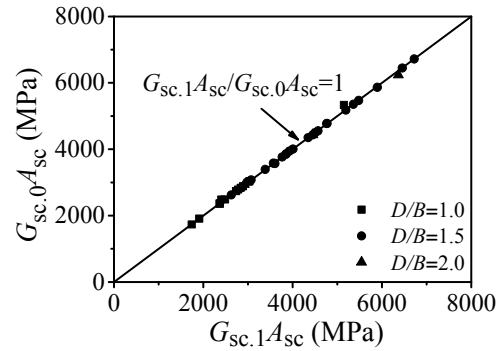

 Fig. 13 Comparison of the  $\tau$ - $\gamma$  curve for CFT column and the corresponding core concrete


Fig. 14 Comparison between the finite element values and the formula values of the composite shear stiffness of CFT columns

$$T = T_s + T_c \quad (4)$$

where:  $T_u$  is the ultimate bearing capacity of rectangular CFT columns,  $T_s$  and  $T_c$  are the ultimate torsional strength of the HST and the core concrete respectively. The shear stress at steel tube under pure torsion was constant along the thickness direction of steel plate. Then according to thin wall plate torsional strength calculation, following equation was obtained.

$$T_s = 2A_{s0}t_s\tau_s \quad (5)$$

where:  $A_{s0}$  is the area enclosed by the centerline of steel plates, and  $\tau_s$  is the average shear stress of the steel tube at ultimate state. Then based on material strength theory, the relation between  $\tau_s$  and  $f_s$  can be expressed as follows.

$$\tau_s = f_s / \sqrt{3} \quad (6)$$

Fig. 15 shows the shear stress distribution at the core concrete of a typical example. The shear stress varied approximately linear from the center to the outer side. Then the shear stress was conservatively assumed as linear, and the ultimate torsional strength of core concrete can be

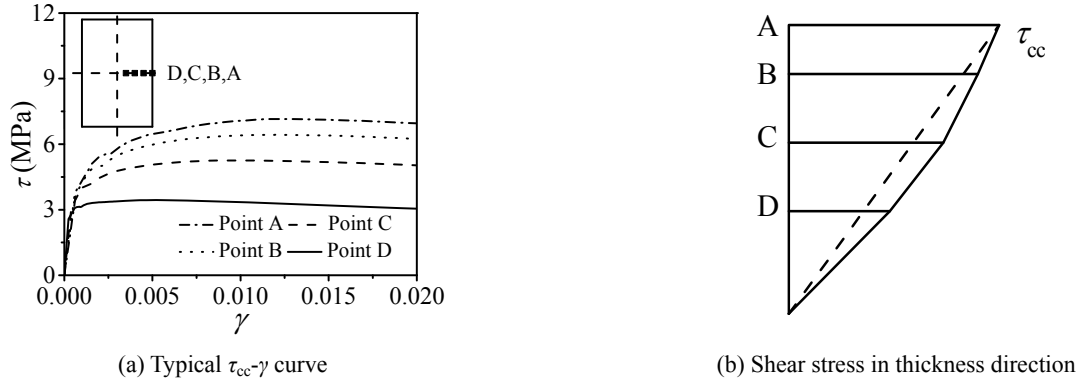


Fig. 15 The shear stress distribution of the core concrete

expressed as

$$T_c = \alpha h_c b_c^2 \tau_{cc} \tag{7}$$

where:  $h_c$  is section height and  $b_c$  is section width of the core concrete,  $\alpha$  is a coefficient related to the D/B (Liu

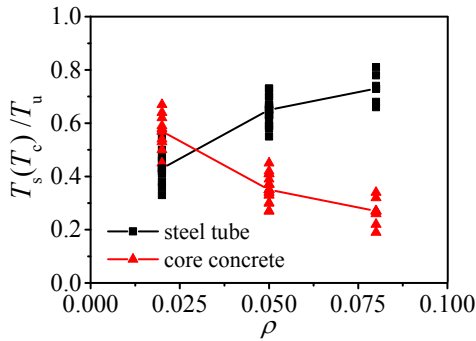


Fig. 16 Torsional moment proportion of the steel tube and the core concrete respective

2017). Together with Eqs. (4)-(7), the torsional strength calculation formula for rectangular CFT column could be obtained as

$$T_u = 1.15 A_{so} t_s f_s + \alpha h_c b_c^2 \tau_{cc} \tag{8}$$

To be clearer about the torque share between steel tube and the core concrete, and the relations to steel ratio, Fig. 16 gives the torsional moment sharing percentages at the steel tube and the core concrete. Results indicated that the torque share at the encased steel tube increased as the rise of steel ratio, and  $T_s/T_u$  varied nearly linearly from 0.4-0.8. Under 0.02 steel ratio, the torque share at steel tube in some cases were even lower than that at core concrete. And when under the same steel ratio, other factors, namely the depth-width ratio, steel yield strength and the concrete strength, presented minimum effect on the torque share, with a results distraction within 15%.

### 3.3.2 Design code comparison

In order to validate the effectiveness of proposed formula, the ultimate torsion strength that obtained from FE

Table 2 Proposed formulas of torsional ultimate bearing capacity

Number	Formulas	Ref.
1	$T_u = r_t W_{sc} \tau_{scy}$ $\tau_{scy} = (0.455 + 0.313\alpha^{2.33}) \xi f_{scy}; r_t = 1.431 + 0.242 \ln \xi$	Han <i>et al.</i> (2007b)
2	$T_u = W_T f_{sv}$ $W_T = \pi r_0^3 / 2; \pi r_0^2 = DB$	GB 50936-2014 (2014)

Table 3 Comparisons between the tested results and the predicted result

Specimens	D/mm	B/mm	$f_s$ /MPa	$f_{cu}$ /Mpa	t/mm	$T_{u,c}$ /kN·m	L/mm	$T_{u,c}/T_{u,e}$			
								FE	Eq. (8)	Eq. (9)	Eq. (10)
S-T	200	200	261.4	39	4.5	69.59	1620	1.06	1.08	1.24	0.94
R1-T	200	150	261.4	39	4.5	48.84	1620	1.03	1.13	1.25	0.89
R2-T	200	100	354.8	39	4.5	37.05	1620	1.03	1.03	1.12	1.13
FC	123.5	123.5	274	25.6	4.5	23.52	1590	1.06	1.06	1.06	1.32
Average								1.05	1.05	1.17	1.07
Coefficient dispersion								0.01	0.04	0.08	0.17

models and the formula calculations were obtained and plotted in Fig. 17. The average value of  $T_{u,1}/T_{u,0}$  was 1.05 with a variation coefficient of 0.03, which confirming the precision of the proposed Eq. (8). Table 2 lists the calculation formulas of pure torsional capacity of CFT column in related researches and design codes, and Table 3 presents the comparison between tested results ( $T_{u,c}$ ) and the FE results ( $T_{u,0}$ ) versus the calculated strengths. The average value of  $T_{u,c}/T_{u,0}$  was 1.01 with the coefficient dispersion as 0.07, and the average value of  $T_{u,c}/T_{u,1}$  was 1.05 with a coefficient dispersion as 0.04. Figs. 18 and 19 show the comparison of Eq. (9) ( $T_{u,2}$ ) with the FE results ( $T_{u,0}$ ), and with the calculations form Eq. (8) ( $T_{u,1}$ ). It can be seen that Eq. (9) was close to the Eq. (8) proposed in this paper and the FE results, but was more conservative than the Eq. (8). Then Eq. (8) can well predict the torsional strength with the highest accuracy, when comparing to theoretical values.

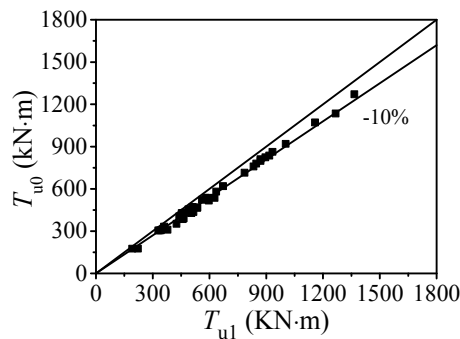


Fig. 17 Comparisons of FE results and predicted results using Eq. (8)

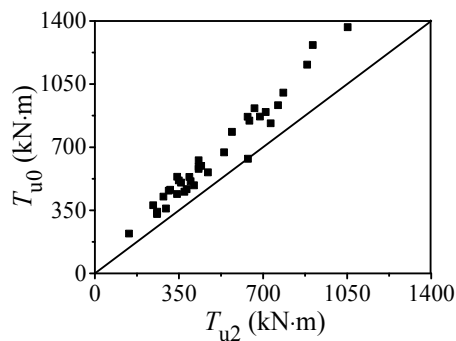


Fig. 18 Comparison between the Eq. (9) and the FE results

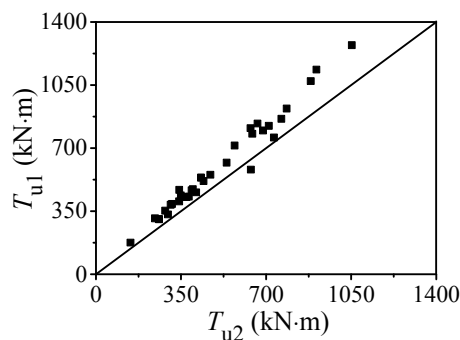


Fig. 19 Comparison between the Eq. (9) and the Eq. (8)

## 4. Conclusions

In this paper, the pure torsion simulations of 39 rectangular CFT columns were performed, and parametric studies were conducted to get further understanding on the torsion problems of rectangular CFT columns. Then a modified torsional strength formula for rectangular CFT columns was proposed, and the effectiveness was verified with test data, numerical results and other design codes. Based on the studies and analysis, the following conclusions could be drawn:

- The full-scale FE models with more precise material constitutive relations were established and validated. Then with the verified FE models, the parameters were performed. And results indicated that the steel yield strength, the steel ratio and depth-width ratio could all presented influence on the  $T$ - $\gamma$  curve.
- Compared with the plain concrete column, the shear stress at core concrete would be elevated by 18%-48% due to the confinement effect from the steel tube and the cover plate. Then both torsional strength share and ductility at core concrete were greatly improved. Based on the parametric studies, the calculation formula of  $\tau_{cc}$  was presented.
- Based on the superposition principle, a torsional strength calculation formula for rectangular CFT columns was proposed. And the accuracy was validated by test data and the FE simulation results.

## Acknowledgments

This research work was financially supported by the National Key Research Program of China, Grant No.2017YFC0703404, the National Natural Science Foundation of China, Grant No.51578548, and Hunan Province Preeminence Youth Fund, Grant NO.2019JJ20029.

## References

- Abed, F., AlHamaydeh, M. and Abdalla, S. (2013), "Experimental and numerical investigations of the compressive behavior of concrete filled steel tubes (CFSTs)", *J. Struct. Eng.*, **80**, 429-439.
- Aslani, F., Uy, B., Wang, Z.W. and Petal, A. (2016), "Confinement models for high strength short square and rectangular concrete-filled steel tubular columns", *Steel Compos. Struct., Int. J.*, **22**(5), 937-974.
- Beck, J. and Kiyomiya, O. (2003), "Fundamental Pure Torsional Properties of Concrete Filled Circular Steel Tubes", *J. Mater. Concrete Struct. Pavements*, **60**(739), 285-296.
- CECS28-2012, China Standard (2012), Technical specification for concrete-filled steel tubular structures, China Planning Press; Beijing, China.
- Chen, Y.W. (2003), "Research on torsion and section behavior of concrete-filled steel tubular columns", Master Dissertation; National Central University, Taiwan.
- Ding, F.X., Ying, X., Zhou, L. and Yu, Z.W. (2011), "Unified calculation method and its application in determining the uniaxial mechanical properties of concrete", *Frontiers Architect. Civil Eng. China*, **5**(3), 381.
- Ding, F.X., Fu, Q., Wen, B., Zhou, Q. and Liu, X. (2018),

- “Behavior of circular concrete-filled steel tubular columns under pure torsion”, *Steel Compos. Struct., Int. J.*, **26**(4), 501-511.
- Evirgen, B., Tuncan, A. and Taskin, K. (2014), “Structural behavior of concrete filled steel tubular sections (CFT/CFSt) under axial compression”, *Thin-Wall. Struct.*, **80**(7), 46-56.
- GB 50936-2014, China Standard (2014), Technical Code for Concrete Filled Steel Tubular Structures, China Construction Industry Press; Beijing, China.
- Gong, A. (1989), *Experimental Study on Concrete Filled Steel Tubular Short Column under Combined Torsion and Compression*, Beijing Institute of Civil Engineering and Architecture, Beijing, China.
- Han, L.H., Yao, G.H. and Tao, Z. (2007a), “Behaviors of concrete-filled steel tubular members subjected to combined loading”, *Thin-Walled Structures*, **45**(6), 600-619.
- Han, L.H., Yao, G.H. and Tao, Z. (2007b), “Performance of concrete-filled thin-walled steel tubes under pure torsion”, *Thin-Wall. Struct.*, **45**(1), 24-36.
- Hassanein, M.F. and Kharoob, O.F. (2014), “Analysis of circular concrete-filled double skin tubular slender columns with external stainless steel tube”, *Thin-Wall. Struct.*, **79**(6), 23-27.
- Kim, J.K., Kwak, H.G. and Kwak, J.H. (2013), “Behavior of Hybrid Double Skin Concrete Filled Circular Steel Tube Columns”, *Steel Compos. Struct., Int. J.*, **14**(14), 191-204.
- Kim, W.W., Mum, J.H. and Yang, K.H. (2015), “Simplified model for the stress-strain relationship of confined concrete”, *Steel Compos. Struct., Int. J.*, **31**(4), 79-86.
- Kitada, T.N.H. (1991), “Experimental Study on Ultimate Strength of Concrete-filled Square Steel Short Members Subjected to Compression or Torsion”, *Proceedings of Inter. Confer. on Steel-Concrete Composite*, Fukouka, Japan, September.
- Lai, M.H. and Ho, J.C.M. (2014), “Confinement effect of ring-confined concrete-filled-steel-tube columns under uni-axial load”, *Eng. Struct.*, **67**(5), 123-141.
- Lee, E.T., Yun, B.H., Shim, H.J., Chang, K.H. and Lee, G.C. (2009), “Torsional Behavior of Concrete-Filled Circular Steel Tube Columns”, *J. Struct. Eng.*, **135**(10), 1250-1258.
- Liu, H.W. (2017), *Mechanics of Materials, Higher Education Press*, Beijing, China.
- Mashiri, F.R., Uy, B., Tao, Z. and Wang, Z.B. (2014), “Concrete-filled VHS-to-steel fabricated section stub columns subjected to axial compression”, *J. Constr. Steel Res.*, **95**(4), 141-161.
- Moon, J., Roeder, C.W. and Lehman, D.E. (2012), “Analytical modeling of bending of circular concrete filled steel tubes”, *Eng. Struct.*, **42**(7), 58-66.
- Nie, J.G., Wang, Y.H. and Fan, J.S. (2012), “Experimental study on seismic behavior of concrete filled steel tube columns under pure torsion and compression-torsion cyclic load”, *J. Constr. Steel Res.*, **79**(1), 115-126.
- Patel, V.I., Uy, B., Prajwal, K.A. and Aslani, F. (2016), “Confined concrete model of circular, elliptical and octagonal CFST short columns” *Steel Compos. Struct., Int. J.*, **22**(3), 497-520.
- Park, J.W. and Choi, S.M. (2013), “Structural behavior of CFRP strengthened concrete-filled steel tubes columns under axial compression loads”, *Steel Compos. Struct., Int. J.*, **14**(5), 453-472.
- Uenaka, K. and Tsunokake, H. (2016), “Concrete filled elliptical steel tubular members with large diameter-to-thickness ratio subjected to bending”, *Structures*, **5**(2), 58-66.
- Wang, Y.H. (2013), “Study on Torsion Effect in Concrete Filled Steel Tube Piers of Curved Girder Bridges”, Ph.D. Dissertation; Tsinghua University, Beijing, China.
- Wang, Y.H., Nie, J.G. and Fan, J.S. (2016), “A new model for analyzing nonlinear torsion behavior of concrete filled steel tube columns with rectangular section”, *Earthq. Eng. Eng. Vib.*, **15**(2), 269-282.
- Xiamuxi, A. and Akira, H. (2011), “Compression text of RCFT columns with thin-walled steel tube and high strength concrete”, *Steel Compos. Struct., Int. J.*, **11**(5), 391-402.

CC

**Nomenclature**

$\sigma_{cp}$	Interaction stress
$f_{cu}$	Compressive cubic strength of concrete
$f_{scy}$	Nominal yielding strength of the composite sections subjected to axial compression
$f_{sv}$	Design value of shear strength
$f_s$	Yield strength of steel tube
$T$	Torsional moment
$T_s$	Ultimate moment shared by steel tube
$T_c$	Ultimate moment shared by concrete
$T_u$	Ultimate bearing capacity
$\tau$	Shear stress
$\tau_u$	Ultimate shear stress
$\tau_s$	Shear stress of steel tube
$\tau_{scy}$	Nominal yielding strength of the composite sections subjected to pure concrete
$\tau_c$	Shear stress of plain concrete
$\tau_{cc}$	Shear stress of core concrete
$\gamma$	Shear strain
$\gamma_{sc,u}$	Ultimate shear strain
$D$	Section height
$B$	Section width
$L$	Length of CFT members
$t$	Wall thickness of the steel tube
$D/B$	Depth-width ratio
$h_c$	Section height of core concrete
$b_c$	Section width of core concrete
$G_{sc}$	Shear modulus of CFT members
$G_s$	Shear modulus of steel
$G_c$	Shear modulus of concrete
$A_{sc}$	Section area
$A_s$	Area of steel tube
$A_c$	Area of core concrete
$A_{so}$	Areas made by the average thickness of steel tube
$W_{sc}$	Torsional section factor
$\rho$	Steel ratio of columns ( $=A_s/A_{sc}$ )
$\xi$	Confinement factor
$r_t$	Nominal torisonal yield strength ratio